Photochemistry and Photobiology, 20**, **: *–*

Modulation of Optical Properties of Dissolved Humic Substances by their Molecular Complexity†

Ricardo A. Mignone[1], Marcela V. Martin[2], Faustino E. Morán Vieyra[1], Valeria I. Palazzi[1], Beatriz López de Mishima[1], Daniel O. Mártire[2] and Claudio D. Borsarelli*[1]

[1]Laboratorio de Cinética y Fotoquímica, Instituto de Química del Noroeste Argentino (INQUINOA, CONICET), Universidad Nacional de Santiago del Estero, Santiago del Estero, Argentina
[2]Instituto de Investigaciones Fisicoquímicas Teóricas y Aplicadas (INIFTA, CONICET/UNLP), Facultad de Ciencias Exactas, Universidad Nacional de La Plata, La Plata, Argentina

Received 1 December 2011, accepted 28 February 2012, DOI: 10.1111/j.1751-1097.2012.01135.x

ABSTRACT

In this study, we show that several UV–Vis absorbance, steady-state and time-resolved fluorescence parameters of a series of dissolved humic substances (DHS) from different sources (*e.g.* terrestrial fulvic and humic acids, and humic acid-like molecules extracted from composted and vermicomposted wastes) correlate with the molar absorptivity at 280 nm per mole of organic carbon (ε_{280}), which in turn is proportional to the molecular complexity (*e.g.* molecular size, aromaticity and oxidation degree) of the DHS. Both absorbance and fluorescence spectral responses were sensitive to the molecular complexity associated with the maturation degree of the DHS. Depending on the DHS, different emitting responses by excitation at the UVA (340 nm) and VIS (460 nm) regions of the absorption spectra were observed. The results were explained in terms of the extent of intramolecular electronic interactions between electron donor groups, such as polyhydroxylated aromatics and indoles, and more oxidized acceptor groups (*e.g.* quinones or other oxidized aromatics) as the molecular complexity of the DHS increased.

INTRODUCTION

Humic substances (HS) are ubiquitous in the environment, where they are formed during the microbiological and abiotic transformations of animal and plant materials. They are complex macromolecules, which have a yellow to black appearance, and are acidic and generally heterogeneous (1). The chemical composition and functional structure of the HS depend on geological and environmental conditions where they were originated. The main elements that compose HS are carbon, hydrogen, oxygen and small amounts of nitrogen and occasionally phosphorous and sulfur, which form polymeric aromatic, phenolic and heterocyclic structures that contain carboxylic groups and nitrogen functionalities. Operationally, HS are classified by their aqueous solubility with pH. Humic acid (HA) is the fraction of HS that is not soluble in water under acidic conditions (pH $<$ 2), but is soluble at higher pH, with average molecular weight of 3–5 kDa, approximately. Fulvic acid (FA) is the fraction that is soluble at all pH values, with average molecular weight less than 1–2 kDa. Finally, the completely insoluble fraction at all pH is called Humin (HU), which is an important soil component. Therefore, dissolved humic substances (DHS) mainly as FA and HA are found in natural waters as components of the total dissolved organic matter (DOM), where their interaction with light has important consequences in environmental biology and chemistry.

The UV–Vis absorption spectra of DHS decreases exponentially with increasing wavelength (2–4), providing to aquatic organisms protection from damaging UV radiation, and modulating the color of superficial waters. Although the optical properties of DHS and DOM from different sources have been investigated for a long time by both absorption and fluorescence spectroscopy (2–18), the structural basis of these properties remains unclear, as a result of the complex and diverse composition of the HS depending on their origin and/or source.

Recently, Del Vecchio *et al.* (15–17) proposed a model of optical properties of DHS, in which the absorption and emission spectra of the macromolecules arise from a very large number of absorbing and emitting states, where intramolecular electronic interactions between donor–acceptor chromophores play an important role.

In the present study, we studied absorption and fluorescence spectral properties of a series of DHS ranging from FA standards, partially oxidized HA-like compounds extracted from composted and vermicomposted domestic solid wastes, and HA from peat and farm soils. We found that several absorption and emission parameters obtained by spectral fitting and/or analysis correlated with the molecular complexity of the DHS (*i.e.* molecular size, aromaticity and oxidation degree) represented by the molar absorptivity at 280 nm per mole of organic carbon (ε_{280}). UV spectral fitting and complementary potentiometric acid–basic titrations also confirmed the formation of more oxidized substituent groups with the increases of the molecular size and/or maturation degree of the DHS. Steady-state and time-resolved fluorescence spectroscopy performed with both UVA (340 nm) and VIS (460 nm) excitation, confirmed the existence of a set of absorbing and emitting species that increased with the molecular

†This paper is part of the Special Issue on the 21st IAPS Winter Conference in Mendoza, Argentina.

*Corresponding author email: cborsarelli@yahoo.com.ar (Claudio D. Borsarelli)

complexity of the DHS, resulting in progressive redshifts of the absorption and emission spectra, due to enhanced intermolecular charge-transfer processes. The present results strongly support the previous assessment that visible absorption and emission features of DHS are originated from charge-transfer interactions between hydroxyl (methoxy)-aromatic electron donors and carbonyl (quinoid-like) electron acceptors in the backbone of the DHS (15–18).

MATERIALS AND METHODS

Materials. Soil fulvic acids Waskish Peat (WPFA) and Pony Lake (PLFA) were from IHSS (International Humic Substance Society) and used as received. Terrestrial peat humic acid from Aldrich (AHA) and Fluka (FHA) were purified by precipitation with HCl and separated from impurities by filtration and redissolved with NaOH (19,20). Humic acid sample from a soil (SHA) of a horticultural farm of Santiago del Estero was kindly gifted by Prof. M.I. Sánchez de Pinto of the Experimental Composting Plant of the University of Santiago del Estero. Humic acid-like substances from composted domestic solid waste material were obtained as previously reported (8). A brief description of the extraction and purification of these HA-like materials is given in the Supporting Material. In the case of the composting process, two compost samples were separated after 45 days and 10 months of initiating the process, respectively, which after extraction of HA-like materials were the samples C45D and C10M, respectively. In addition, a fraction of the fresh compost obtained after 45 days was separated and inoculated with Californian earthworms *Eisenia foetida* during extra 11 months, and the HA-like substance extracted was labeled as VC11M.

Methods. The total organic carbon (TOC) was measured with a high-temperature carbon analyzer (model TOC-500; Shimadzu Corp., Kyoto, Japan) using a calibration curve of potassium biphtalate as standard, before each analysis to check for instrumental shifts.

The content of total carboxylic (R-COOH) and phenolic (φ-OH) functional groups of the DHS was estimated by potentiometric acid–base titrations according the method proposed by Campitelli *et al*. (21). Details can be found in the Supporting Information. Briefly, titrations in the pH range of 3.0–10.5 were performed at least three times to ensure reproducibility under nitrogen atmosphere to avoid CO_2 interference. The charge developed by the humic substance molecule Q_{HS} (meq/g_{HS}) as a function of pH was calculated, and the modified multimodal affinity distribution Eq. (1) was used to describe the specific binding of proton to DHS (22), where Q_i is the charge associated (meq/g_{HS}) with the acidic *i-th* group with $pK_{a,i}$ as the association proton constant, and n_i is the width of the affinity distribution.

$$Q_{HS} = Q_{min} + \sum_i \frac{Q_i \times 10^{n_i(pH-pK_{a,i})}}{1 + 10^{n_i(pH-pK_{a,i})}} \quad (1)$$

Fitting of Eq. (1) was performed using the Microcal Origin® 8.5 software (OriginLab Corp., Northampton, MA), as shown in Fig. S1. The content of total (aliphatic + aromatic) carboxylic groups (R-COOH) was estimated as the ΣQ_i for species with $pK_a < 8$, whereas Q_i with $pK_a > 8$ was accounted for phenolic-like acidic groups (see Table S1).

Before spectroscopic characterization, all samples were filtered through 0.45 μm Millipore membrane filters (EMD Millipore, Billerica, MA) to minimize scattering effects by insoluble small particles. Stationary UV–Vis absorbance spectra were obtained with a Hewlett-Packard 8453 diode array spectrophotometer (Agilent Technologies, Santa Clara, CA). Fluorescence spectra were recorded with a Hitachi F-2500 (Hitachi High-Technologies Corp., Kyoto, Japan) instrument using excitation and emission slit width of 5 nm. Fluorescence quantum yields of the DHS with excitation wavelengths at 340 and 460 nm (Φ_F^{DHS}) were determined by actinometry using as references quinine sulfate in 1 *N* H_2SO_4 ($\Phi_F = 0.57$) and fluorescein in NaOH 0.1 *N* ($\Phi_F = 0.95$) in aqueous solutions, respectively (23). The Φ_F^{DHS} was calculated by comparison of the integrated fluorescence intensity of the DHS and reference solutions matched in absorbance (≈0.05) at the excitation wavelength to avoid inner filter effects. The same refractive index for both DHS and reference solution was considered.

Contour maps of excitation-emission matrix (EEM) spectra were obtained recording the emission spectra between 350 and 600 nm by keeping a constant 5 nm excitation step from 250 to 500 nm. Both excitation and emission slit width was 5 nm. The EEM spectra were processed using the Microcal Origin® 8.5 software (OriginLab Corp.).

Fluorescence decays were obtained by the time-correlated single photon counting technique with a Tempro-01 apparatus of Horiba Jobin Yvon (Glasgow, UK), using as excitation pulse sources ultrafast Nanoled® at 340 (±15)nm or 460 (±27)nm operating at 1 MHz (Horiba Jobin Yvon, Glasgow, UK). The time resolution of the system was approximately 55 ps and the emission bandwidth was selected at 12 nm. All fluorescence decays were monitored at room temperature and under air-saturated aqueous solutions. The fluorescence intensity decays were deconvoluted from the pulse excitation response at 340 nm or 460 nm using the Fluorescence Decay Analysis Software DAS6® of Horiba Jobin Yvon; and the fluorescence intensity decay was fitted with the multiexponential model function Eq. (2), where n is the number of single exponential decays, τ_i and α_i are the decay time and the fluorescence intensity amplitude at $t = 0$ of each decay, respectively.

$$I(t) = \sum_{i=1}^{n} \alpha_i \exp(-t/\tau_i) \quad (2)$$

In all cases, up to $n \leq 4$ (including a prompt scattering component) was used in the fitting Eq. (2) to obtain satisfactory fits ($\chi^2 \approx 1.0 \pm 0.2$) of the decay curves (see Fig. S2). The average lifetime τ_{av} was calculated with Eq. (3), where f_i is the fractional contribution of each decay time to the steady-state intensity (23).

$$\tau_{av} = \sum_{i=1}^{n} f_i \tau_i = \frac{\sum_{i=1}^{n} \alpha_i \tau_i^2}{\sum_{i=1}^{n} \alpha_i \tau_i} \quad (3)$$

Time-resolved emission spectra (TRES) by excitation at 340 or 460 nm were also obtained in air-saturated solutions of approximately 10 mg·L^{-1} DHS at 25°C, by collecting counts during 200 s for each decay time using the TRES automatic routine of the DAS6® software. The spectra were recorded with wavelength steps of 5 nm and emission bandwith of 12 nm. The slices of TRES ($I(\lambda, t)$) at different times were constructed from the deconvoluted fluorescence decay function using the global exponential fitting analysis routine of the DAS6® software to obtain the wavelength-dependent pre-exponential factor $\alpha_i(\lambda)$ associated with τ_i decay time. This procedure minimizes the noise contribution in the TRES at the end of the decay time. Time-resolved area normalized emission spectroscopy (TRANES), $I_N(\lambda, t)$, were obtained with Eq. (4), by area normalization of each slide of TRES ($I(\lambda, t)$), to match the spectral area at time t with that of $t = 0$, according to the method proposed by Koti *et al*. (24).

$$I_N(\lambda, t) = \frac{\int I_0(\lambda) d\lambda}{\int I_t(\lambda) d\lambda} I(\lambda, t) \quad (4)$$

RESULTS AND DISCUSSION

UV–Vis spectral properties correlate with molecular complexity of DHS

The UV–Vis absorbance spectra of the DHS were nearly featureless and decreased monotonically with increasing wavelength, as typically observed for this type of material (2–9, 15–18). The lack of vibronic structure in the UV–Vis spectra of DHS is the consequence of the overlapping of absorption bands of a wide variety of different chromophoric species present in the macromolecule. For a quantitative spectral

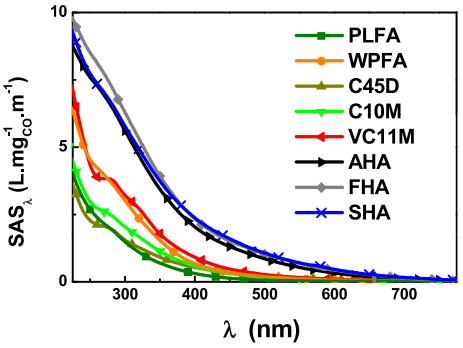

Figure 1. Dissolved organic carbon normalized UV–Vis spectrum of 50 mg L^{-1} dissolved humic substances from different sources: humic substance abbreviations: PLFA, Pony Lake fulvic acid; WPFA, Waskish Peat fulvic acid; C45D, 45 days-old domiciliary compost humic acid-like; C10M, 11 months-old humic acid-like; VC11M, 11 months-old vermicomposted humic acid-like; AHA, purified Aldrich humic acid; FHA, purified Fluka humic acid; SHA, farm soil humic acid.

comparison, the UV–Vis spectrum (A_λ) of each DHS was normalized to its TOC content and presented as specific absorbance spectrum (SAS_λ), as calculated with Eq. (5) (5–7,25), Fig. 1.

$$SAS_\lambda(L \cdot mg_{OC}^{-1} \cdot m^{-1}) = \frac{A_\lambda}{TOC(\%wt/wt) \times C_{HS}(g \cdot L^{-1}) \times b(cm)} \times 10 \quad (5)$$

The intensity of the SAS_λ of the DHS series can be grouped according to the origin of the samples. For instance, the lowest SAS_λ values in the whole spectral range were observed for the domiciliary composts (*i.e.* C45D and C10M) and for the Pony Lake fulvic acid (PLFA), whereas vermicomposted VC11M and the Waskish Peat fulvic acid (WPFA) showed intermediate values, and all terrestrial humic acids AHA, FHA and SHA the highest ones. Hur *et al.* (5) showed that the intensity of the SAS_λ of DHS mixtures composed by Suwannee River fulvic acid (SRFA) and Aldrich humic acid (AHA) was proportional to the relative amount of AHA. This result confirmed that the increment of the average molecular size of the DHS increases the intensity of SAS_λ. Our results corroborate this tendency, as FA- and HA-like compounds from compost are molecules with smaller molecular weight than stabilized HA (6). Besides the molecular mass of the DHS, other factors can increase the specific absorbance, such as the formation of more extended π-conjugated bonds systems and/or oxidation of functional groups of the aromatic moieties (2,8–10,17,18). This effect can be better understood by analyzing the specific ultraviolet absorbance values at 254 and 280 nm (*i.e.* $SUVA_{254}$ and $SUVA_{280}$, respectively) from the SAS_λ (7–9). These wavelengths are normally chosen because most $\pi \rightarrow \pi^*$ electron transitions for phenolic substances, aniline derivatives, benzoic acids, polyenes and polycyclic aromatic hydrocarbons, which are precursors or components of certain types of HS, occur in this region of the UV range. These parameters are currently used for classification and/or characterization of DHS, yielding important clues regarding the degree of aromaticity, source functions, oxidation degree and possibly molecular weight (2,5–10,25).

Table 1 shows that the highest $SUVA_{254}$ and $SUVA_{280}$ values were obtained for the humic acid samples AHA, FHA and SHA, indicating that this DHS contains the largest degree of aromaticity and conjugated double bonds in its structure, as expected from highly stabilized soils HS (4,6). Conversely, the lowest values of SUVAs were obtained for C45D, according with its lower maturity degree expected for a HA-like extracted from fresh composted material. In addition, the SAS_λ of the C45D and VC11M samples showed an absorbance shoulder at $\lambda \approx 280$ nm, which can be related to the presence of quinone and lignin-like chromophores (26) and/or aromatic amino acid residues such as Trp and Tyr from protein components in the starting waste material (2). As the maturity of the composted material increased, *e.g.* C10M, the shoulder at 280 nm almost vanished in the spectrum probably by the overlapping of charge-transfer absorption transitions bands produced by the increment of more oxidized groups (17,18). In the case of vermicomposted material VC11M this shoulder persisted, probably because of a larger content of peptide or protein-like compounds produced during the composting by the earthworms (27).

On the other hand, the product of the $SUVA_{280}$ by the factor 120 yields the molar absorptivity at 280 nm per mole of organic carbon (ε_{280} [=] $L \cdot mol_{CO}^{-1} \cdot cm^{-1}$), which was proposed as a useful parameter for the estimation of an operational molecular weight of humic substances MW_{HS} according to the empirical linear relationship Eq. (6) (6),

Table 1. Some physicochemical and UV–Vis absorption properties of dissolved humic substances (DHS) of different sources in aqueous media at 25°C.

		$SUVA_{254}$	$SUVA_{280}$				$-RCO_2H^d$	$-\varphi$-OH§
DHS*	TOC (% wt/wt)	($L \cdot m^{-1} \cdot mg_{OC}^{-1}$)		$MW_{HS}^‡$ (Da)	E_4/E_6	A_{ET}/A_{Bz}	(meq/g_{HS})	
PLFA	52.5†	2.56	1.96	1428	10.51	0.11	4.87	2.03
WPFA	53.6†	4.40	3.68	2254	8.89	0.16	7.05	1.74
C45D	62.2	2.20	1.96	1428	5.54	0.11	5.84	2.96
C10M	66.5	2.85	2.48	1679	9.23	0.35	4.84	1.01
VC11M	48.0	4.09	3.81	2313	7.77	0.27	4.43	1.87
AHA	44.1	7.45	6.53	3614	6.81	1.04	6.05	1.43
FHA	40.0	8.34	7.28	3977	5.57	0.90	6.70	0.51
SHA	41.2	7.56	6.65	3674	6.03	0.67	5.59	1.47

*Humic substance abbreviations: PLFA, Pony Lake fulvic acid; WPFA, Waskish Peat fulvic acid; C45D, 45 days-old domiciliary compost humic acid-like; C10M, 10-months old domiciliary compost humic acid-like; VC11M, 11-months domiciliary vermicomposted humic acid-like; AHA, purified Aldrich humic acid; FHA, purified Fluka humic acid; SHA, soil humic acid from horticultural farm of Santiago del Estero, Argentina; †from IHSS http://www.ihss.gatech.edu/elements.html; ‡MW_{HS} calculated with Eq.(6); §calculated with Eq. (2); all SD < 2%.

$$MW_{HS} = 490 + 3.99 \times \varepsilon_{280} \quad (6)$$

This empirical relationship was obtained from aquatic and soil sources of DHS spanning a molecular weight range between 0.8 and 4.1 kDa, whose weight-average molecular weights were obtained by high-pressure size exclusion chromatography (HPSEC; 6). Therefore, assuming that most DHS possess molar absorptivities and molecular weights within the confines of Eq. (6), this relationship can be used judiciously to provide approximate MW_{HS} in the absence of other interfering chemical substances, such as metal oxides and organic dyes.

Table 1 shows that the calculated MW_{HS} for DHS series of this study are comprised into the molecular weight range of the empirical Eq. (6), with good agreement for the value of AHA, whose reported MW of 4100 and 3070 kDa measured by high-pressure size exclusion chromatography (HPSEC; 6) and field flow fractionation (FFF; 28), respectively. Thus, it can be concluded that the SUVA analysis combined with the empirical Eq. (6) yields an approximate trend of MW_{HS} of the DHS in the order FHA > SHA ≈ AHA > VC11M > WPFA > C10M > PLFA ≈ C45D.

A similar conclusion can be obtained from the analysis of the absorbance ratio at two different wavelengths in the visible region, *e.g.* 465 and 665 nm (namely E_4/E_6 ratio), which has been widely used for the characterization and classification of DHS, being normally larger for FA than for HA (29). Thus, it has been long considered that this parameter correlates inversely with the molecular size and/or the formation of multiring aromatic systems in the DHS (6,7,29,30). The increases of molecular complexity of DHS by formation of more extended and oxidized aromatic systems is expected to decrease the E_4/E_6 due to the relative increment of the extinction coefficient in the red region of the visible spectrum (29,31). Table 1 shows the calculated E_4/E_6 values follow the trend: PLFA > C10M > WPFA > VC11M > AHA > SHA > FHA ≈ C45D. Except for C45D, this E_4/E_6 trend can be also explained by increment of molecular size and aromaticity, in agreement with the SUVA's analysis discussed elsewhere. However, for the composted C45D, depending on the spectral region selected, *i.e.* UV ($SUVA_{280}$) or Vis regions (E_4/E_6), opposite conclusions about its maturation degree can be obtained. In this case, the lower E_4/E_6 value of C45D could be associated with the presence of nonHS impurities, such as organic dyes with strong red-light absorbance, which were present in the domiciliary waste and coextracted together with the HA-like substances, contributing to the anomalous decrease of E_4/E_6. With the advance of the composting process, these impurities are biodegraded and the E_4/E_6 ratio is only given by the absorbance values of the DHS, such as the case of the extracted HA-like from more composted sample C10M. Consequently, the structural and/or maturation degree conclusions obtained by UV–Vis spectral analysis of DHS from composted samples can strongly depend on the spectral region selected and/or sample origin and treatment, and therefore the combination of two or more spectral parameters should be necessary for its characterization.

Despite of the lack of defined absorption maxima, useful extra information related with the type and relative amount of oxidized substituent groups on benzenoid chromophores of the DHS can be obtained by UV spectral fitting with Eq. (7), assuming that the UV spectrum of DHS is composed of three types of Gaussian-shaped bands called locally excited (LE), benzenoid (Bz) and electron-transfer (ET; 3).

$$A = \sum_i A_i \exp\left[-\left(\frac{2(\ln 2)^{1/2}(E - E_i)}{\Delta_i}\right)^2\right] \quad (7)$$

In Eq. (7) the suffix i identifies the LE, Bz or ET bands; A_i, E_i and Δ_i are the absorbance, the energy value corresponding to the maximum wavelength (in eV), and the full width at half maximum (FWHM) of each absorption band, respectively. The intensity (A_i) of the ET band is largely affected by the presence of polar functional groups on the benzene ring, whereas the benzenoid band Bz is almost unaffected (3). As a result, the ratio A_{ET}/A_{Bz} calculated for model compounds increased from 0.03 (benzene ring), to 0.25–0.35 for phenolic compounds, and above 0.40 for aromatic rings with carbonyl and carboxylic groups (32). Recently, we reported that during the composting of domiciliary waste residues, the A_{ET}/A_{Bz} ratio of the extracted HS-like increased up to values corresponding to aromatic carboxylic groups, indicating the increment of the oxidation degree of the DHS with evolution of the composting process (8). Thus, this ratio can be a useful tool for a comparative characterization of the substitution and oxidation degree of the aromatic chromophores in DHS. Figure 2 shows the fitting with Eq. (7) of the UV spectra of PLFA and AHA samples. In all cases, satisfactory fittings were obtained only considering the contribution of Bz and ET bands, since the LE band is shifted to the far UV. The fitting recovered A_i,

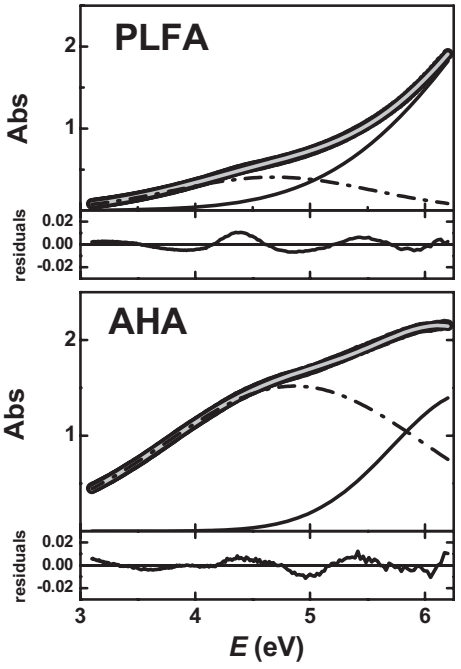

Figure 2. Fitting with Eq. (7) of the UV spectra of 50 mg·L^{-1} Pony Lake fulvic acid and purified Aldrich humic acid in aqueous solution at neutral pH. The solid gray line represents the spectral fit, and the black dashed and solid lines are the respective benzenoid and electron-transfer recovered bands. The spectral fitting residuals are represented below.

E_i and Δ_i values for all DHS are presented in Table S2 and the calculated A_{ET}/A_{Bz} ratio is collected in Table 1. Figure 3 shows that the A_{ET}/A_{Bz} ratio increased with ε_{280} of the DHS, indicating that the number of oxidized substituent groups on benzenoid chromophores increases with the molecular size of the DHS. For instance, both fulvic acids PLFA and WPFA, and the fresh compost C45D have $A_{ET}/A_{Bz} < 0.25$, in agreement with lower molecular complexity and/or oxidation degree. As the composting process advances, the A_{ET}/A_{Bz} ratio increased to 0.35 and 0.27 for C10M and VC11M, respectively, reflecting a slight increase of oxidized chromophores. Instead, the terrestrial humic acids SHA, FHA and AHA showed $A_{ET}/A_{Bz} > 0.6$, which is typical of well-stabilized humic acid derived of soil sources containing more oxidized aromatic chromophores, such as carboxylic acids and quinone-like groups (32).

The increment on the oxidation degree in the DHS was also tested by potentiometric acid–base titration curves (see Table S1 and Fig. S1), that allowed the estimation of the total content (meq/g_{HS}) of (aliphatic + aromatic) carboxylic (R-COOH, p$K_a \approx 3$–7) and phenolic-like (φ-OH, p$K_a > 8$) substituents, by fitting of the proton affinity curves with Eq. (1). The results are collected in Table 1, and it can be observed that the relative amount of R-COOH is approximately 70–90% larger than φ-OH groups, signifying that major anionic charge contribution is due to acidic groups. Interestingly, the relative amount of phenolic to carboxylic groups, *i.e.* the ratio φ-OH/R-COOH, decreased proportionally with the apparent molecular size of the DHS (*i.e.* $\varepsilon_{280} \propto MW_{HS}$), Fig. 3. This variation was parallel with the increment of the A_{ET}/A_{Bz} ratio, confirming the evolution of less-oxidized phenolic-like groups to more oxidized carboxylic and/or quinone-like groups with the increment of the maturation degree and/or molecular size of the HS (5,33,34).

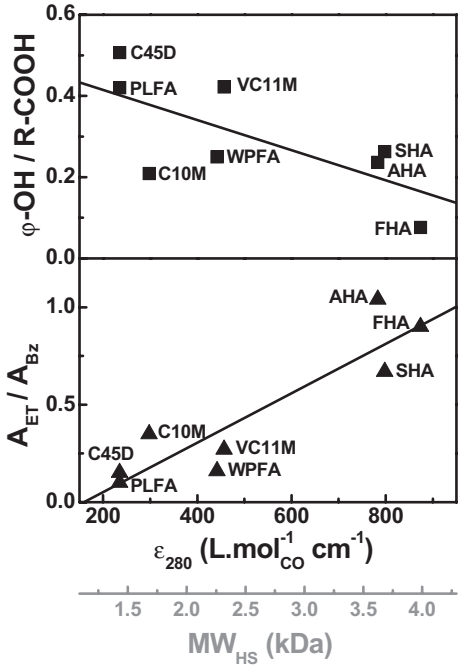

Figure 3. Relationship between the specific molar absorptivity (ε_{280}) of the dissolved humic substances with (top) the molar ratio between phenolic and carboxylic groups (φ-OH/R-COOH) and (bottom) the absorbance ratio A_{ET}/A_{Bz} calculated from fitting of UV spectrum of DHS with Eq. (7). The MW_{HS} x-scale (gray line) calculated with Eq. (6) is also shows for comparison. DHS abbreviations as in Fig. 1.

Intra- but not intermolecular electronic interactions govern the fluorescence behavior of DHS

The spectral fluorescence emission properties of all DHS were independent of the concentration used in the study (≤50 mg·L^{-1}), indicating the lack of aggregation effects and/or of specific interactions between fluorophores of different HS molecules in this concentration range. Nevertheless, the excitation and emission spectra of DHS were dependent on both the excitation and monitoring emission wavelengths, respectively, as expected for multifluorophoric molecules (see Fig. S3). In these cases, the stationary fluorescence spectral analysis is better understood performing EEM spectroscopy of DHS (8,12,13), Fig. 4. It can be observed that each DHS showed different normalized EEM, which represent a precise three-dimensional emission fingerprint of the samples. The evaluation of the EEM indicated a progressive spectral change from fulvic acids (PLFA and WPFA) to humic acid AHA, with intermediary behavior for the composted samples (C45D, C10M and VC11M).

The excitation-emission maxima pairs $(\lambda_{ex}/\lambda_{em})_{EEM}$ of the EEM are presented in Table 2. The $(\lambda_{ex}/\lambda_{em})_{EEM}$ of the fulvic acids PLFA and WPFA were placed at 310/358 nm and 339/468 nm, respectively, which indicates the presence of different types of fluorophores in each fulvic acid. It is noteworthy that the EEM of the freshly composted sample C45D showed two excitation-emission maxima pairs, *e.g.* $(\lambda_{ex}/\lambda_{em})_{EEM1}$ = 277/352 nm and $(\lambda_{ex}/\lambda_{em})_{EEM2}$ = 318/445 nm, which were very similar to those reported for DHS extracted from fresh corn composted sample (13). Furthermore, these maxima pairs are in the same range as those for each standard PLFA and WPFA, Table 2. The origin of the blue shifted emission in the EEM of C45D can be associated with tyrosine, tryptophan or phenolic-like residues (11,14),

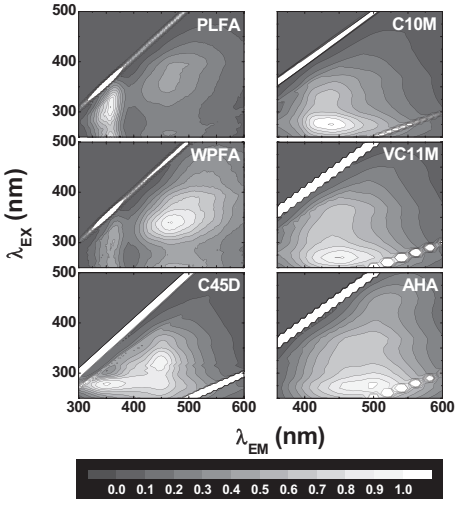

Figure 4. Normalized excitation-emission matrix for dissolved humic substances in aqueous solutions at neutral pH, divided into 10 equal-value contour intervals. DHS abbreviations as in Fig. 1.

Table 2. Fluorescence properties of dissolved humic substances (DHS) of different sources in aqueous media at 25°C.

		Ex 340 nm				Ex 460 nm			
DHS	EEM $(\lambda_{ex}/\lambda_{em})_{EEM}$	$\Phi_F \times 10^3$	λ_{em}^{max} (nm)	τ_{av}^{450} (ns)	τ_{av}^{600} (ns)	$\Phi_F \times 10^3$	λ_{em}^{max} (nm)	τ_{av}^{500} (ns)	τ_{av}^{600} (ns)
PLFA	310/358	15.6	430	4.72	4.15	5.9	524	4.39	3.57
WPFA	339/468	5.3	450	4.55	3.70	3.0	525	4.53	3.70
C45D	277/352 318/445	1.5	450	4.26	2.74	1.1	520	3.12	2.33
C10M	275/438	4.1	440	3.05	3.09	1.9	515	4.04	3.43
VC11M	271/450	2.3	445	3.35	2.91	1.4	515	4.29	3.49
AHA	275/499	2.9	478	3.79	4.02	2.1	520	4.70	4.30
FHA	270/506	1.9	495	4.10	4.23	2.5	515	4.92	4.21
SHA	278/507	3.2	500	3.80	4.10	3.9	515	4.44	3.71

DHS abbreviations as in Table 1.

present in the soluble microbial degradation products formed during the mineralization phase of composting (2). Conversely, the red-shifted band in the EEM of C45D can be related to the presence of aromatic groups with electron acceptor substituents, *e.g.* quinones and carboxylic groups (35). Interestingly, these two bands in the EMM of C45D collapsed in a single band at $(\lambda_{ex}/\lambda_{em})_{EEM}$ = 275/438 nm for the more matured compost C10M, which is a value closer to the region defined for HS-like (14). The vermicomposted sample VC11M showed slightly more redshifted in emission $(\lambda_{ex}/\lambda_{em})_{EEM}$ = 271/450 nm, probably by the presence of oxidized chromophores due to the intense composting with the earthworms. Finally, for the well-stabilized peat and soil HA (AHA, FHA and SHA) the larger emission redshift of the EEM maxima was observed, *e.g.* $(\lambda_{ex}/\lambda_{em})_{EEM} \approx$ 275/500 nm. Furthermore, together with the redshifting of the emission maxima, the EEM of the DHS showed a progressive broadening of the matrix contour map in the order C45D < PLFA < C10M < VC11M ≈ WPFA < AHA ≈ FHA ≈ SHA.

Figure 5 shows the variation of both the emission maximum (λ_{em}) and full width at the half maximum (FWHM) obtained by excitation at 340 and 460 nm, respectively, with the specific molar absorptivity (ε_{280}) of the DHS. Clearly, only by excitation at the blue edge of the absorbance spectra of DHS, both λ_{em} and FWHM values increased monotonically with the apparent molecular size of the DHS. In effect, the emission spectrum of DHS shifted to the red approximately 70 nm together with a spectral width enlargement of about 1500 cm^{-1} from PLFA to SHA. On the contrary, excitation at 460 nm does not modify appreciably the emission spectral shape among the DHS series, with emission maxima around 525 nm and much more narrow bands (FWHM ≈ 3700 cm^{-1}). These results suggest that excitation at 340 nm populates more red-edge-emitting states as the molecular complexity of the DHS increases, whereas by excitation at 460 nm produces excited states with similar emitting properties for all DHS.

In fact, the fluorescence quantum yield of the DHS obtained at both excitation wavelengths, *i.e.* Φ_F^{340} and Φ_F^{460}, showed a complex dependence, Table 2. The fulvic acids PLFA and WPFA showed larger Φ_F^{λ} values ($\approx 10^{-2}$), according to their lesser complex composition and smaller molecular sizes (4). Nevertheless, the variation of Φ_F^{λ} with the excitation wavelength was dependent on the origin of the DHS. For example, Φ_F^{λ} decreased with λ_{ex} for FA, but the opposite effect was observed for HA, Table 2. Furthermore, the fluorescence

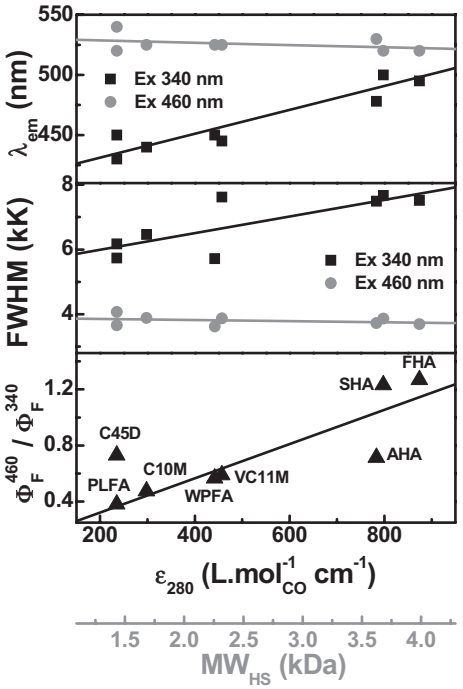

Figure 5. Variation of fluorescence emission maximum (λ_{em}), full width at half maximum and quantum yield ratio ($\Phi_F^{450}/\Phi_F^{360}$) as a function of the specific molar absorptivity (ε_{280}) of the dissolved humic substances (DHS). The MW_{HS} x-scale (gray line) calculated with Eq. (6) is also shows for comparison. DHS abbreviations as in Fig. 1.

quantum yield ratio ($\Phi_F^{460}/\Phi_F^{340}$) increased monotonically from 0.38 to 1.25 with ε_{280}, Fig. 5, indicating an enlargement of the fluorescence efficiency of the red-absorbing fluorophores with the molecular size of the DHS.

The dynamic fluorescence behavior of the DHS was also complex. In all cases, multiexponential fluorescence decays were observed and fitted with Eq. (2) (see Fig. S2), with lifetimes τ_i and amplitude α_i values dependent on both the excitation and monitoring emission wavelengths. The average lifetime (τ_{av}) was calculated with Eq. (3), as it represents a useful parameter to provide a simpler way of illustrating the overall decay variations. Figure 6a shows the changes of τ_{av} with the emission wavelength obtained by excitation at 340 and 460 nm, respectively. For the fulvic acids PLFA and WPFA and the less composted C45M, excitation at 340 nm

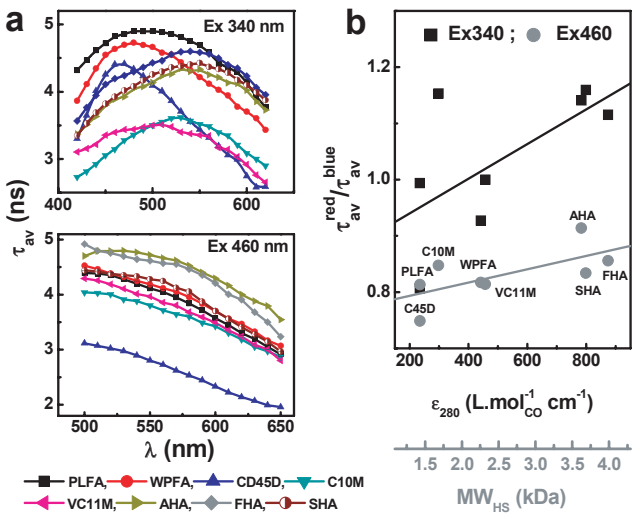

Figure 6. (a) Variation of the average lifetime (τ_{av}) with the emission wavelength observed by excitation of the dissolved humic substances (DHS) at 340 and 460 nm, respectively. (b) Relationship between the specific molar absorptivity (ε_{280}) of the DHS for the ratio between red- and blue-edge average lifetimes ${\tau_{av}}^{600}/{\tau_{av}}^{450}$ with excitation at 340 nm (■), and ${\tau_{av}}^{600}/{\tau_{av}}^{500}$ with excitation at 460 nm (●).

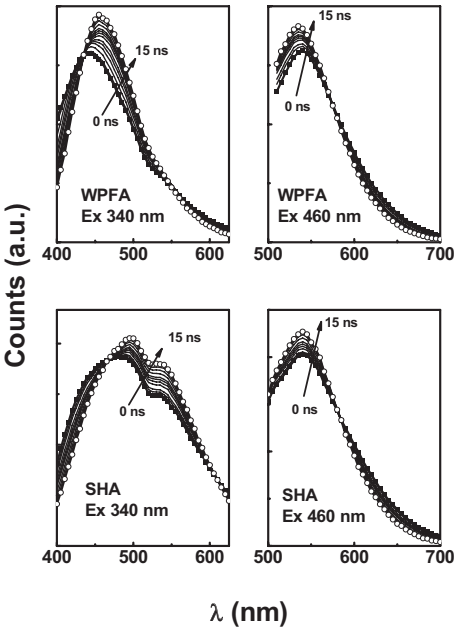

Figure 7. Time-resolved area normalized emission spectra of Waskish Peat fulvic acid and soil humic acid obtained between 0 (■) and 15 ns (○) after excitation at 340 and 460 nm, respectively.

produced a maximum τ_{av} value at emission wavelength < 500 nm. Instead, HA samples showed the highest τ_{av} at emission wavelengths around 550 nm. Table 2 presents pairs of τ_{av} values monitored at the blue and red edge of the emission spectra of the DHS for each excitation wavelength. Apparently, no correlation with the origin of DHS can be observed. However, only the ratio between the lifetimes in the red and blue edges of the emission spectrum obtained by excitation at 340 nm, *i.e.* $({\tau_{av}}^{600}/{\tau_{av}}^{450})_{Ex340}$, increased with the apparent molecular size with of the DHS, Fig. 6b. This behavior could reflect that the blue-edge emitting species are more efficiently quenched by intermolecular processes with the increment of the molecular complexity of the DHS. Conversely, excitation at 460 nm produced a progressive diminution of τ_{av} with the emission wavelength, indicating faster relaxation processes of the red-edge fluorophores, as it was previously reported for several aquatic HS (16). The poor dependence of $({\tau_{av}}^{600}/{\tau_{av}}^{500})_{Ex460}$ ratio with ε_{280} in this case, Fig. 6b, suggests again that visible excitation of the DHS generates excited states with similar emission properties independently of the type and source of the macromolecule.

Finally, different dependence with the excitation wavelength was observed for the evolution of the time-resolved area normalized emission spectra (TRANES) of the DHS, which were calculated from the experimental TRES with Eq. (4) (24). The advantage of TRANES is to overcome the prior knowledge of the number of fluorescent species in the ground state required in the standard kinetic interpretation of TRES. This requirement is difficult to fulfill in complex molecular systems, such as multifluorophoric molecules. Instead, in TRANES no assumptions of any ground or excited-state kinetics are necessary, with the extra advantage that the presence of isoemissive points in the spectra supports any model that involves two or more emitting species in the sample (24).

Upon UVA excitation (340 nm), the initial TRANES ($t = 0$) was dependent on the nature of DHS, being more blueshifted and narrow for FA than HA, as showed for WPFA and SHA in Fig. 7 (see Fig. S4 for the others' DHS). In all cases, as the blue-edge species decayed, the emission maximum shifted to the red until approximately the wavelength value observed in the steady-state fluorescence spectrum of each DHS, together with the parallel growth of the relative intensity of the red-emitting species and the presence of at least two isoemissive points (λ_{ie}). Under this condition, the spectral redshifting of the emission maxima of the TRANES ($\Delta\lambda_t$) obtained by UVA excitation was proportional to the apparent molecular size, *i.e.* ε_{280} (Fig. S5).

On the contrary, excitation at 460 nm produced similar TRANES for all DHS, with almost the same emission maxima as in the stationary fluorescence spectra (≈530 nm). In this case, the evolution of TRANES showed a small narrowing without significant spectral shifts, together with the increment of the relative intensity at the emission maximum. In this case, a single isoemissive point (λ_{ie}) at the red edge of the TRANES was observed. The position of this λ_{ie} also shifted to the red with the apparent molecular size of the DHS, Fig. S5. The analysis of the dynamic behavior of the TRANES indicated that the apparent lifetime for the interconversion of the blue- and red-shifted excited state species τ_{ic} (Table S3) is a few ns longer than the observed average lifetime at the same emission wavelenght, τ_{av}. This result agrees with a parallel decay model of the excited states by both radiative and charge-transfer pathways, *i.e.* $({\tau_{av}}^{-1} = {\tau_{rad}}^{-1} + {\tau_{ic}}^{-1})$.

All the other results suggest that intramolecular electronic interactions increase with the molecular complexity of the DHS. The present results completely agree with the model proposed by Del Vecchio *et al.* (15–17), who described that the optical properties of aquatic FA and HA arise from a near continuum of intramolecular absorbing and emitting

charge-transfer states formed by donor moieties groups such as polyhydroxylated aromatics and indoles, and more oxidized acceptor groups (*e.g.* quinones or other oxidized aromatics) rather than solely from a simple summation of the spectra of numerous electronically isolated chromophores. In this framework, the increment of the A_{ET}/A_{Bz} ratio together with diminution of φ-OH/R-COOH ratio with ε_{280} (Fig. 3), confirms the progressive formation of oxidized aromatic moieties in the DHS that can act as charge-transfer acceptor partners in the macromolecule. Furthermore, both stationary and dynamic emission results (Figs. 4–7) with excitation at 340 nm indicated the formation of higher energy locally excited states, which decay directly to their ground state or intramolecular charge-transfer excited states responsible for the large Stoke's shift observed by UVA excitation. The amount of these donor–acceptor charge-transfer states increases with the molecular size and/or maturation degree (aromaticity, oxidation of functional groups, etc.) of the DHS, as demonstrated by the increments of the $\Phi_F{}^{460}/\Phi_F{}^{340}$ and $(\tau_{av}{}^{600}/\tau_{av}{}^{450})_{Ex340}$ ratios with ε_{280} (Figs. 5 and 6). The changes on the TRANES under UVA excitation confirmed the prompt formation of high-energy locally excited donor states that decays to lower energy emitting states (Fig. 7).

On the other hand, excitation at 460 nm induced the formation of excited states with similar emitting properties independently of the DHS. As denoted by Del Vecchio *et al.* (15,16), the red shifted fluorescence at >475 nm can be attributed to recombinational emission arising from direct excitation of low energy charge-transfer states. As the molecular size and oxidation degree of the DHS increases, the number of these charge-transfer states also increases allowing efficient exciton coupling.

In summary, we showed through steady-state and dynamic spectroscopic parameters that the increment of aromaticity and/or oxidation extent on DHS modulates their optical properties in a controlled fashion due to the enlargement of donor–acceptor charge-transfer interactions.

Acknowledgements—The authors thank the Argentinean Funding Agencies CICyT-UNSE, CONICET and ANPCyT (PICT-06-01090) for their financial support. R.A.M and M.V.M. thanks CONICET for a doctoral fellowship. CDB thanks also the Alexander von Humboldt Foundation for a Georg Foster Fellowship.

SUPPORTING INFORMATION

Additional Supporting Information may be found in the online version of this article:

Table S1. Fitting parameters obtained with Eq. (S2) for the curves of charge developed by the humic substance molecule Q_{HS} (meq/g_{HS}) against pH (see Fig. S2).

Table S2. Recovered fitting parameters of UV spectra of DHS using Eq (S3).

Table S3. Spectral redshift emission maxima of the TRANES ($\Delta\lambda_t$), isoemissive points (λ_{ie}) and decay time of interconversion (τ_{ic}) for DHS at different excitation wavelength.

Figure S1. Curves of charge developed, Q_{HS} (meq/g_{HS}) against pH (solid circles) of N_2-bubbled solutions of 8 mg of purified Aldrich humic acid (AHA) and 11-months vermicomposted humic acid-like (VC11M) at 25°C. The solid red line represents the data fitting with Eq. (S1). The fitting residuals are represented below.

Figure S2. Fluorescence decay curves of air-saturated 10 mg·L^{-1} DHS solutions obtained with excitation at 340 nm and emission at 450 nm. Emission bandwith 12 nm.

Figure S3. Excitation and emission fluorescence spectra of air-saturated 10 mg·L^{-1} DHS solutions. Excitation and emission slits width 5 nm.

Figure S4. Time-resolved area normalized emission spectra (TRANES) of DHS obtained between 0 (black line) and 15 ns (dark gray line) after excitation at 340 and 460 nm, respectively.

Figure S5. Relationship between the specific molar absorptivity (ε_{280}) of the dissolved humic substances (DHS) with: the emission maxima shift between the final and initial TRANES, $\Delta\lambda(t)$, at both excitation wavelengths (*e.g.* 340 and 460 nm); and with the TRANES isoemissive wavelength, λ_{ie}, observed by excitation at 460 nm. The MW_{HS} x-scale (gray line) calculated with Eq. (5) is also shows for comparison. DHS abbreviations as in Fig. 1.

Please note: Wiley-Blackwell is not responsible for the content or functionality of any supporting information supplied by the authors. Any queries (other than missing material) should be directed to the corresponding author for the article.

REFERENCES

1. Davies, G. and E. A. Ghabbour (1998) *Humic Substances. Structure, Properties and Uses*, pp. 1–259. Royal Society of Chemistry (RSC), Cambridge.
2. Domeizel, M., A. Khalil and P. Prudent (2004) UV spectroscopy: a tool for monitoring humidification and proposing an index of the maturity of compost. *Biores. Technol.* **94**, 177–184.
3. Korshin, G. V., C.-W. Li and M. M. Benjamin (1997) Monitoring the properties of natural organic matter through UV-spectroscopy: a consistent theory. *Water Res.* **31**, 1787–1795.
4. Senesi, N., T. M. Miano, M. R. Provenzano and G. Brunetti (1989) Spectroscopic and compositional comparative characterization of I.H.S.S. reference and standard fulvic and humic acids of various origins. *Sci. Total Environ.* **81/82**, 143–156.
5. Hur, J., M. A. Williams and M. A. Schlautman (2006) Evaluating spectroscopic and chromatographic techniques to resolve dissolved organic matter via end member mixing analysis. *Chemosphere* **63**, 387–402.
6. Chin, Y. P., G. Alken and E. O'Loughlin (1994) Molecular weight, polydispersity, and spectroscopic properties of aquatic humic substances. *Environ. Sci. Technol.* **28**, 1853–1858.
7. Uyguner, C. S. and M. Bekbolet (2005) Implementation of spectroscopic parameters for practical monitoring of natural organic matter. *Desalination* **176**, 47–55.
8. Morán Vieyra, F. E., V. Palazzi, M. Sanchez de Pinto and C. D. Borsarelli (2009) Combined UV–Vis absorbance and fluorescence properties of extracted humic substances-like for characterization of composting evolution of domestic solid wastes. *Geoderma* **151**, 61–67.
9. He, X., B. Xi, Z. Wei, X. Guo, M. Li, D. An and H. Liu (2011) Spectroscopic characterization of water extractable organic matter during composting of municipal solid waste. *Chemosphere* **82**, 541–548.
10. Marhuenda-Egea, F. C., E. Martinez-Sabater, J. Jorda, R. Moral, M. A. Bustamante, C. Paredes and M. D. Perez-Murcia (2004) Dissolved organic matter fractions formed during composting of winery and distillery residues: evaluation of the process by fluorescence excitation-emission matrix. *Chemosphere* **68**, 301–309.
11. Coble, P. G. (1996) Characterization of marine and terrestrial DOM in seawater using excitation-emission matrix spectroscopy. *Mar. Chem.* **51**, 325–346.

12. Sierra, M. M. D., M. Giovanela, E. Parlanti and E. J. Soriano-Sierra (2005) Fluorescence fingerprint of fulvic and humic acids from varied origins as viewed by single-scan and excitation/emission matrix techniques. *Chemosphere* **58**, 715–733.
13. Hunt, J. F. and T. Ohno (2007) Characterization of fresh and decomposed dissolved organic matter using excitation-emission matrix fluorescence spectroscopy and multiway analysis. *J. Agric. Food Chem.* **55**, 2121–2128.
14. Chen, W., P. Westerhoff, J. A. Leenheer and K. Booksh (2003) Fluorescence excitation-emission matrix regional integration to quantify spectra for dissolved organic matter. *Environ. Sci. Technol.* **37**, 5701–5710.
15. Del Vecchio, R. and N. V. Blough (2004) On the origin of the optical properties of humic substances. *Environ. Sci. Technol.* **38**, 3885–3891.
16. Boyle, E. S., N. Guerriero, A. Thiallet, R. Del Vecchio and N. V. Blough (2009) Optical properties of humic substances and CDOM: relation to structure. *Environ. Sci. Technol.* **43**, 2262–2268.
17. Ma, J., R. Del Vecchio, K. S. Golanoski, E. S. Boyle and N. V. Blough (2010) Optical properties of humic substances and CDOM: effect of borohydride reduction. *Environ. Sci. Technol.* **43**, 2262–2268.
18. Maurer, F., I. Christl and R. Kretzschmar (2010) Reduction and reoxidation of humic acid: influence on spectroscopic properties and proton binding. *Environ. Sci. Technol.* **44**, 5787–5792.
19. Saito, T., L. K. Koopal, W. H. van Riemsdijk, S. Nagasaki and S. Tanaka (2004) Adsorption of humic acid on goetita: isotherms, charge adjustments, and potential profiles. *Langmuir* **20**, 689–700.
20. Andjelkovic, T., J. Perovic, M. Purenovic, S. Blagojevic, R. Niklic, D. Andjelkovic and A. Bojic (2006) A direct potentiometric titration study of the dissociation of humic acid with selectively blocked functional groups. *Ecletica Quím.* **31**, 39–46.
21. Campitelli, P. A., M. I. Velasco and S. B. Ceppi (2003) Charge development and acid-base characteristics of soil and compost humic acids. *J. Chil. Chem. Soc.* **48**, 91–96.
22. Iglesias, A., R. Lopez, D. Gondar, J. Antelo, S. Fiol and F. Arce (2009) Effect of pH and ionic strength on the binding of paraquat and MCPA by soil fulvic and humic acids. *Chemosphere* **76**, 107–113.
23. Lakowicz, J. R. (1999) *Principles of Fluorescence Spectroscopy*, pp. 53–54. Kluwer Academics, New York.
24. Koti, A. S. R., M. M. G. Krishma and N. Periasamy (2001) Time-Resolved area-normalized emission spectroscopy (TRANES): a novel method for confirming emission from two excited states. *J. Phys. Chem. A* **105**, 1767–1771.
25. Potter, B. B. and J. C. Wimsatt (2005) Determination of total organic carbon and specific UV absorbance at 254 nm in source water and drinking water. USA Environmental Protection Agency. EPA Document EPA/600/R-05/055. 415.3–1–415.3–56.
26. Rivero, C., T. Chirenje, L. Q. Ma and G. Martinez (2004) Influence of compost on soil organic matter quality under tropical conditions. *Geoderma* **123**, 355–361.
27. Campitelli, P. A. and S. Ceppi (2008) Effects of composting technologies on the chemical and physicochemical properties of humic acids. *Geoderma* **144**, 325–333.
28. Beckett, R., Z. Jue and J. C. Giddings (1987) Determination of molecular weight distributions of fulvic and humic acids using flow field-flow fractionation. *Environ. Sci. Technol.* **21**, 289–295.
29. Chen, Y., N. Senesi and M. Schnitzer (1977) Information provided on humic substances by E4-E6 ratios. *Soil Sci. Soc. Am. J.* **41**, 352–358.
30. You, S.-J., Y. Yin and H. E. Allen (1999) Partitioning of organic matter in soils: effects of pH and water/soil ratio. *Sci. Total Environ.* **227**, 155–160.
31. Lguirati, A., G. Ait Baddi, A. El Mousadik, V. Gilard, J. C. Revel and M. Hafidi (2005) Analysis of humic acids from aerated and non-aerated urban landfill composts. *Int. Biodeter. Biodegr.* **56**, 8–16.
32. Scott, A. I. (1964) *Interpretation of the Ultraviolet Spectra of Natural Products*. Pergamon Press, New York.
33. Spaccini, R. and A. Piccolo (2007) Molecular characterisation of compost at increasing stages of maturity. I: chemical fractionation and infrared spectroscopy. *J. Agric. Food Chem.* **55**, 2293–2302.
34. Velasco, M. I., P. A. Campitelli, S. B. Ceppi and J. Havel (2004) Analysis of humic acid from compost of urban wastes and soil by fluorescence spectroscopy. *Agriscientia* **21**, 31–38.
35. Miano, T., G. Sposito and J. P. Martin (1990) Fluorescence spectroscopy of model humic acid type polymers. *Geoderma* **47**, 349–359.